

# Interference of longitudinal and transversal fragmentations in the Josephson dynamics of Bose-Einstein condensates

Anal Bhowmik<sup>1,2,\*</sup> and Ofir E. Alon<sup>1,2</sup>

<sup>1</sup>*Department of Physics, University of Haifa, Haifa 3498838, Israel*

<sup>2</sup>*Haifa Research Center for Theoretical Physics and Astrophysics,  
University of Haifa, Haifa 3498838, Israel*

(Dated: July 13, 2022)

A set-up to investigate Josephson dynamics of interacting bosons in the presence of interference between longitudinal fragmentation, developed during the quantum dynamics, and transversal fragmentation, produced by the geometry of the trap, is proposed. We find and explain how this interference speeds up the collapse of density oscillations and slows down the revival process by analyzing the survival probability along the junction, fluctuations of particle positions across the junction, and the occupancy of the lowest single-particle states. The interference mechanism is always accompanied by a non-trivial transition from loss of coherence to build up of coherence in the first excited single-particle state. Moreover, it is found that a fully fragmented state significantly accelerates the revival process compared to the conventional Bose-Einstein condensate. All in all, we show that the interference of longitudinal and transversal fragmentations establishes new rules for macroscopic tunneling phenomena.

Being a unique state of matter, atomic Bose-Einstein condensates (BECs) have been used as a flexible platform to explore a wealth of physical phenomena, in particular, the Josephson effect [1] which has a prominent manifestation of quantum coherence on a macroscopic scale. Over the years, various exotic features in Josephson junctions of ultracold atoms, such as, Josephson oscillations [2, 3], macroscopic self-trapping [4, 5], collapse and revival sequences [6], matter wave interferometry [7], and squeezing [8, 9] have been investigated. Josephson effects have been observed in complex systems, such as, spinor condensates [10], polariton condensates [11], fermionic superfluids [12], and spin-orbit coupled BECs [13].

In many-particle systems, interactions between the particles lead to correlations and

their manifestation in a BEC is fragmentation which is a widely-studied phenomenon [14–21]. The concept of fragmentation arises when the reduced one-body density matrix starts to have more than one macroscopic eigenvalue in contrast to the conventional BEC with just one macroscopically occupied state. Hitherto, the development of fragmentation has been explored in the atomic Josephson junction only for fully condensed states [22–26]. In recent years, the dynamics of Josephson junctions in two dimensions has been studied taking into account physics that emerges due to the transversal degrees of freedom [27–31].

The transversal degrees of freedom can also enrich the amount of internal correlations in a BEC. This opens the door to ask how correlations impact the Josephson junction. So far, to the best of our knowledge, interference of different fragmentations in a two-dimensional BEC has not been discussed. The question is the following, can we combine the concepts of Josephson junction and different fragmentations which allows to have different internally correlated states, something that one can not produce in one dimension and so far has not been explored. It would allow us to study different channels of fragmentations and how they interfere. It turns out that one of the implications is the tunneling process which becomes complicated when the different fragmentations interfere. Therefore, we propose a set-up to study complicated tunneling processes.

With the emergence of fragmentation as a key perspective of quantum many-body physics, we examine the tunneling dynamics of a plethora of different order of initially fragmented states, and observe an intricate paradigm of tunneling dynamics taking into account the interference of fragmentations. We show that the interference of the fragmentations sets up new rules of the quantum tunneling problem. The rules of tunneling of a fragmented BEC manifests in quantum mechanical quantities, namely, survival probability, build-up of internal coherence, and fluctuations of particles' positions.

The many-body Hamiltonian of  $N$  interacting bosons in two spatial dimensions reads:  $\hat{H}(\mathbf{r}_1, \mathbf{r}_2, \dots, \mathbf{r}_N) = \sum_{j=1}^N [\hat{T}(\mathbf{r}_j) + \hat{V}(\mathbf{r}_j)] + \sum_{j < k} \hat{W}(\mathbf{r}_j - \mathbf{r}_k)$ . Here  $\hat{T}(\mathbf{r}_j)$  is the kinetic energy of  $j$ -th boson and  $\hat{V}(\mathbf{r}_j)$  represents the trap potential.  $\hat{W}(\mathbf{r}_j - \mathbf{r}_k)$  is the inter-boson interaction which is modelled as repulsive Gaussian function [32–34] with  $W(\mathbf{r}_j - \mathbf{r}_k) = \lambda_0 \frac{e^{-(\mathbf{r}_j - \mathbf{r}_k)^2 / 2\sigma^2}}{2\pi\sigma^2}$  where  $\sigma$  is the width of the Gaussian function. Here  $\lambda_0$  is the interaction strength which is related to the interaction parameter  $\Lambda_0 = \lambda_0(N - 1)$ . Throughout this work  $\mathbf{r} = (x, y)$  and the natural units  $\hbar = m = 1$  are employed.

In order to create the different order of fragmented ground states, we design the one-

body trap potential as  $V(x, y) = \frac{1}{2}(x+2)^2 + V(y)$ , where  $V(y) = \frac{1}{2}y^2 + V_L e^{-y^2/8}$ , which transforms from single well to double well potential along the transverse direction as  $V_L$  is increased, see inset in Fig. 1. For the out-of-equilibrium tunneling dynamics, we quench the trap potential from  $V(x, y)$  to  $V'(x, y)$ . The mathematical form of  $V'(x, y)$  for the whole range of  $y$  is  $\frac{1}{2}(x+2)^2 + V(y)$  for  $x < -\frac{1}{2}$ ,  $\frac{1}{2}(x-2)^2 + V(y)$  for  $x > +\frac{1}{2}$ , and  $\frac{3}{2}(1-x^2) + V(y)$  for  $|x| \leq \frac{1}{2}$ . Here, the ramping up of  $V_L$  leads to a four-well trap, see inset in Fig. 2.

We take precedence of the powerful numerical many-body method, the bosonic version of the multiconfigurational time-dependent Hartree method [20, 22, 35–38], also see its multi-layer version for mixtures [39–43]. The method incorporates quantum correlations exhaustively to obtain in-principle numerically exact ground states of different order of initial fragmentations, and the interference of different fragmentation channels in the out-of-equilibrium dynamics.

Our many-body method uses, to obtain the wavefunction, a variationally optimal ansatz which is a linear combination of all permanents generated by distributing the  $N$  bosons over  $M$  time-adaptive orbitals. The many-body wavefunction is described as [36]

$$|\Psi(t)\rangle = \sum_{\{\mathbf{n}\}} C_{\mathbf{n}}(t) |\mathbf{n}; t\rangle, \quad (0.1)$$

where  $C_{\mathbf{n}}(t)$  are the expansion coefficients and  $|\mathbf{n}; t\rangle = |n_1, n_2, \dots, n_M; t\rangle$ . The number of time-dependent permanents  $|\mathbf{n}; t\rangle$  is  $\binom{N+M-1}{N}$ . Here  $M = 1$  boils down to the time-dependent Gross-Pitaevskii equation [44]. As the number of orbitals is increased, convergence of quantities, discussed in this work, with  $M$  is obtained.

In order to accurately capture the many-body physics involved in this work, we have performed the many-body computations with  $M = 8$  time-adaptive orbitals and the convergence are checked with  $M = 10$  time-adaptive orbitals (see the supplemental material [45]). For the numerical solution we use a grid of  $128 \times 128$  points in a box of size  $[-10, 10) \times [-10, 10)$  with periodic boundary conditions. Convergence of the results with the number of grid points has been verified using a grid of  $256 \times 256$  points and presented in [45].

To study the tunneling dynamics of fragmented BECs, we have to classify their basic properties depending on the degree of fragmentations. To remind, the fragmentation here serves as internal structure. In order to identify the condensed or fragmented state, we present the occupation of the first natural orbital,  $n_1$ , as a function of  $V_L$ .  $n_1$  clearly defines

whether the ground state is condensed or fragmented in terms of the loss of coherence in the system. The loss of coherence is determined from diagonalization of the reduced one-particle density matrix  $\rho(\mathbf{r}, \mathbf{r}') = N \int d\mathbf{r}_2 \dots d\mathbf{r}_N \Psi^*(\mathbf{r}', \mathbf{r}_2, \dots, \mathbf{r}_N) \Psi(\mathbf{r}, \mathbf{r}_2, \dots, \mathbf{r}_N)$ . Fig. 1(a) depicts how the ground state loses its coherence as a function of  $V_L$  for two inter-boson interaction strengths  $\Lambda_0 = 0.01\pi$  and  $10\Lambda_0$ . The inter-boson interactions are weak, in the sense that at  $V_L = 0$ , the ground state is more than 99.99% condensed for  $\Lambda_0$  and more than 99.9% condensed for  $10\Lambda_0$ . As is expected, the loss of coherence of the ground state increases with the barrier height, and the ground state becomes 48.55% fragmented for  $\Lambda_0$  and 49.85% fragmented for  $10\Lambda_0$  for  $V_L = 16$ . We find that the ground state becomes two-fold fragmented from about  $V_L \geq 8$ , with the marginally occupied third and fourth orbitals with occupancy around  $10^{-7}$  and the remaining four orbitals have occupancy less than  $10^{-7}$ . The two-fold fragmented ground state indicates that two natural orbitals are macroscopically occupied. For the considered geometry of the trap, the ground orbital is gerade ( $g$ -orbital) and the excited orbital is ungerade ( $u$ -orbital) along the  $y$ -direction. As fragmentation develops the  $g$ - and  $u$ -orbitals tend to be equally occupied. The topology of the investigation indicates that the parity in the  $y$ -direction is a good quantum number. Therefore, we may call this fragmentation, developed by occupying the  $u$ -orbital, the transversal fragmentation.

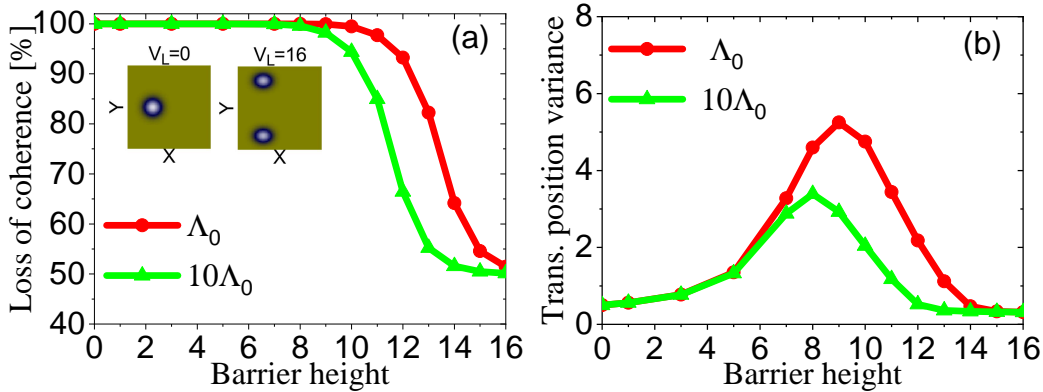


FIG. 1. Initial conditions. (a) Loss of coherence and (b) transversal position variance,  $\frac{1}{N}\Delta_Y^2$ , as a function of the longitudinal barrier height ( $V_L$ ) for two interaction strengths. The inset in panel (a) shows the density per particle for the minimal and maximal  $V_L$ . The number of bosons is  $N = 10$ . We show here dimensionless quantities.

Now, to analyze the distribution of bosons for different order of correlated ground states, we present the many-body transversal position variance,  $\frac{1}{N}\Delta_Y^2 = \frac{1}{N}[\langle\Psi(t)|\hat{Y}^2|\Psi(t)\rangle -$

$\langle \Psi(t) | \hat{Y} | \Psi(t) \rangle^2$ ], in Fig. 1 (b). The motivation is to use this quantity to demonstrate the interference in different fragmentation channels later on in the dynamics. Initially,  $\frac{1}{N} \Delta_Y^2$  monotonously grows with  $V_L$  from the initial value 0.5, i.e., the value for the harmonic potential at  $V_L = 0$ , and reaches its maximal value at about  $V_L = 9$  for  $\Lambda_0$  and  $V_L = 8$  for  $10\Lambda_0$ . Interestingly, due to the appreciable amount of developed transversal fragmentation,  $\frac{1}{N} \Delta_Y^2$  decays and tends to saturates for the maximal  $V_L$ . It is noted that the many-body variances in the longitudinal direction,  $\frac{1}{N} \Delta_X^2$ , are essentially the same for all  $V_L$  with value 0.5 and are practically independent of the interaction strength chosen here (not shown). This suggests a very weak coupling between the  $x$ - and  $y$ -directions of the interacting bosons in the considered two-dimensional double-well trap for all  $V_L$ .

We have prepared different order of transversely fragmented states depending on the value of  $V_L$ . Now, to investigate the interference of fragmentations by generating longitudinal fragmentation, we propose to quench the trap to a four well potential where the bosons tunnel back and forth between the left and right parts of space.

We begin investigating the tunneling dynamics with a basic quantity, namely, the many-body survival probability in the left part of space,  $P(t) = \int_{x=-\infty}^0 \int_{y=-\infty}^{+\infty} d\mathbf{r} \frac{\rho(\mathbf{r}; t)}{N}$ , where  $\rho(\mathbf{r}; t)$  is the density, see in Fig 2(a).  $P(t)$  shows that, although the frequencies of oscillations for different  $V_L$  are essentially the same, due to the practically same Rabi frequency along the  $x$ -direction [45], but the amplitude of oscillations decreases with different rates depending on  $V_L$ . Here we see that for the fully condensed ground state ( $V_L = 1$ ) the amplitude of  $P(t)$  decays and eventually the density collapses. As the state is initially fully condensed, the decay in the amplitude of  $P(t)$  implies the development of longitudinal fragmentation. We find that the decay rate of  $P(t)$  is maximal for  $V_L = 1$  and, as the barrier height gradually increases until  $V_L = 7$ , the decay rate of  $P(t)$  monotonously decreases, although there is no initial transversal fragmentation. This is because the gradual increase of the barrier until  $V_L = 7$  makes the ground state slowly deformed which produces two parts of the ground state along the transverse direction, keeping the coherency of the system unchanged. Therefore, the coherence of the ground state maintains the connection between its two parts along the transverse direction and the decay rate of  $P(t)$  becomes a monotonously decreasing function which decreases as long as the initial transversal fragmentations starts to interfere at  $V_L = 8$ . At  $V_L \geq 8$ , the ground state is already initially transversely fragmented and the connection between the two parts of the ground state starts to be weaker which increases the decay rate

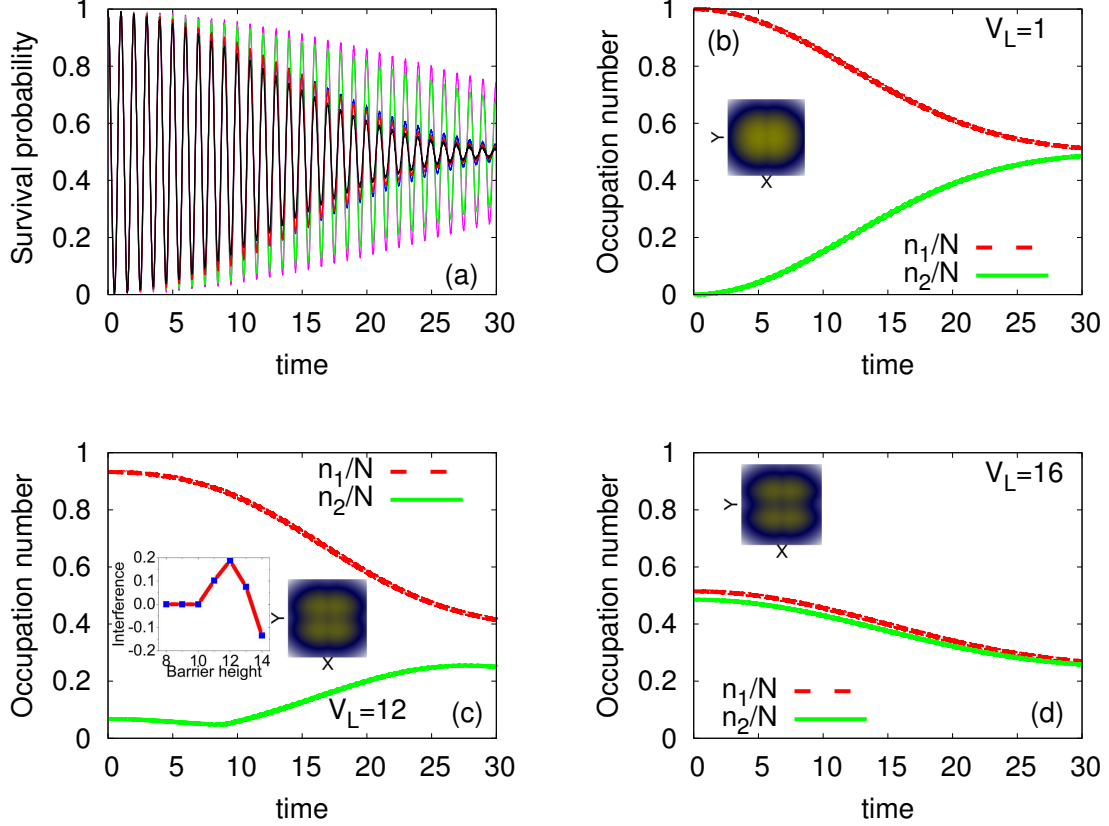


FIG. 2. Tunneling dynamics. (a) Many-body survival probability in the left side of space,  $P(t)$ , for the barrier heights,  $V_L = 1$  (black), 7 (magenta), 10 (green), 12 (red), and 16 (blue) as a function of time. Occupations of the first and second natural orbitals,  $\frac{n_1(t)}{N}$  and  $\frac{n_2(t)}{N}$ , respectively, for (b)  $V_L = 1$ , (c)  $V_L = 12$ , and (d)  $V_L = 16$ . The insets in panels (a), (b), and (c) show the corresponding four-well traps. Also the inset in panel (c) depicts the interference in the intermediate barrier heights from  $V_L = 8$  to  $V_L = 14$ . The inter-boson interaction is  $\Lambda_0$  and the number of bosons  $N = 10$ . We show here dimensionless quantities.

of  $P(t)$ . This speeding up of the collapse of the density oscillations indicates the interference between the longitudinal and transversal fragmentations. Further increase of the barrier height until  $V_L = 12$ , the decay rate of  $P(t)$  monotonously increases, suggesting the increase of the interference between the longitudinal and transversal fragmentations. At  $V_L > 12$ , the density collapse slows down until  $V_L = 16$ , implying that the two parts of the ground state starts to behave like two independent states which means the interference between the longitudinal and transversal fragmentations tends to diminish.

Now, in order to present a clear understanding of the interference of the transversal

and longitudinal fragmentations developed in the process of tunneling, we quantitatively analyze the dynamical occupations of the natural orbitals. Figs. 2 (a), (b), and (c) depict the occupation of the first,  $\frac{n_1(t)}{N}$ , and second,  $\frac{n_2(t)}{N}$ , natural orbitals for  $V_L = 1, 12$ , and 16, respectively. It is found that  $\frac{n_1(t)}{N}$  monotonously decreases, remains as  $g$ -orbital, and eventually tends to saturate for all the initial states, whether the system is fully condensed, partially fragmented, or fully fragmented. Remarkably, the dynamical occupation of the second natural orbital shows intriguing feature. We observe that when the initial state is fully condensed at  $V_L = 1$  (or fully fragmented at  $V_L = 16$ ),  $\frac{n_2(t)}{N}$  monotonously increases (or decreases). For the fully condensed system, the second natural orbital is excited  $g$ -orbital and for the fragmented system, it is  $u$ -orbital. The loss of coherence in the  $u$ -orbital exhibits the system is initially fragmented. Interestingly, in Fig. 2 (c), we find that, initially, the  $u$ -orbital loses its coherence and thereafter the coherence builds up. This transition, from loss of coherence to build up of coherence in the  $u$ -orbital represents the interference of the longitudinal and transversal fragmentations, taking place for intermediate barrier heights from  $V_L = 8$  to  $V_L = 14$ . Moreover, we observe that the  $u$ -orbital loses its coherence until and unless there is a swapping of orders between higher natural orbitals, see [45]. Therefore, the swapping of orders of the orbitals breaks the trend of loss of coherence and build up of coherence in the  $u$ -orbital. To identify at which intermediate barrier height, the maximal interference of the longitudinal and transversal fragmentations occurs, we calculate the difference between the maximal occupancy of the  $u$ -orbital after building up of coherence and its initial occupancy, see the inset in Fig. 2 (c). Positive values of interference in the figure indicates that the build up of coherence in the  $u$ -orbital is more than its initial value. This analysis identifies that the maximal interference of the longitudinal and transversal fragmentations takes place at  $V_L = 12$ .

Now, in order to show the consequences of the interference of the longitudinal and transversal fragmentations on a quantum mechanical observable, we present the time evolution of the many-body  $\frac{1}{N}\Delta_Y^2(t)$  in Fig. 3 (a). As the inter-boson interaction is weak and for  $V_L = 1$  the initial state is fully condensed,  $\frac{1}{N}\Delta_Y^2(t)$  is practically frozen in time due to no interference between the longitudinal and transversal fragmentations. At  $V_L = 7$ , when the ground state is initially depleted (around 0.01%),  $\frac{1}{N}\Delta_Y^2(t)$  shows small oscillations during the tunneling process originating from small interference between the longitudinal and

transversal fragmentations. Increasing of the initial fragmentation in the ground state, say, at  $V_L = 10$ ,  $\frac{1}{N}\Delta_Y^2(t)$  shows oscillatory nature with constant amplitude and frequency of oscillations, due to a stronger interference. Interestingly, at  $V_L = 12$ , we find that  $\frac{1}{N}\Delta_Y^2(t)$  grows as time progresses. This growing nature of  $\frac{1}{N}\Delta_Y^2(t)$  signifies strong coupling of the  $x$ - and  $y$ -directions and it emerges from the very strong interference between the longitudinal and transversal fragmentations. For  $V_L > 12$ ,  $\frac{1}{N}\Delta_Y^2(t)$  slowly tends toward essentially frozen dynamical behavior which exhibits decoupling of the longitudinal and transversal fragmentations.

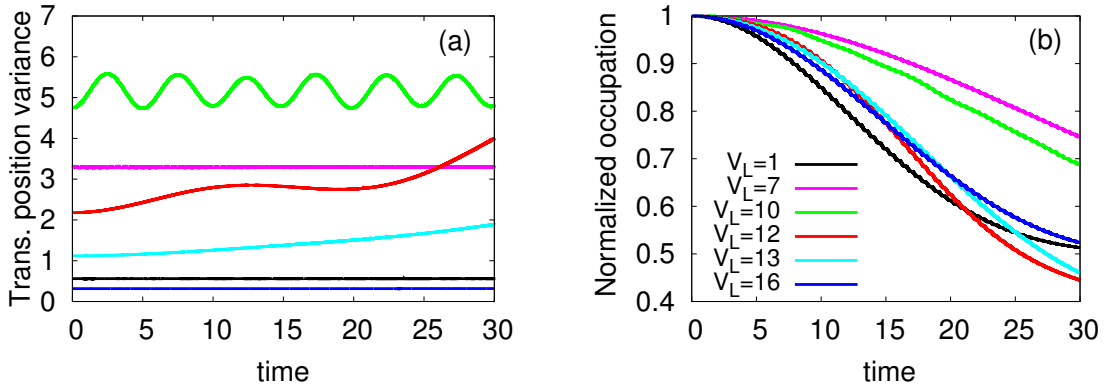


FIG. 3. Interference of longitudinal and transversal fragmentations. (a) Time-dependent transversal position variance per particle,  $\frac{1}{N}\Delta_Y^2(t)$ , and (b) normalized occupation of the  $g$ -orbital,  $\eta(t) = n_1(t)/n_1(0)$ . The inter-boson interaction is  $\Lambda_0$  and the number of bosons  $N = 10$ . Color codes are explained in panel (b). We show here dimensionless quantities.

Now we define a quantity, the normalized condensate fraction,  $\eta(t) = n_1(t)/n_1(0)$ , which can quantify the time-dependent interference between the longitudinal and transversal fragmentations by analysing the real-time rate of the loss of coherence of the  $g$ -orbital, see Fig. 3 (b). As one increases the barrier height from  $V_L = 1$  to  $V_L = 7$ , the rate of decay of  $\eta(t)$  decreases. Further increase of the barrier height, until  $V_L = 12$ , the rate of decay of  $\eta(t)$  increases and, for  $V_L > 12$ , it follows the previous trend of decreasing. If we look into the detail of  $\eta(t)$  for  $V_L = 12$ , we notice that it crosses the corresponding  $\eta(t)$  found at  $V_L = 1, 13$ , and 16 as time progresses and exhibits the maximal rate of loss of coherence. It manifests that the interference between the longitudinal and transversal fragmentations is time dependent. By analysing Fig. 3 (b), we find the following rules: (i) the interference between the



longitudinal and transversal fragmentations speeds up the rate of loss of coherence in the system and (ii) a fully fragmented system, without coupling between the longitudinal and transversal fragmentations, loses coherence with a slower rate compared to the conventional fully condensed BEC.

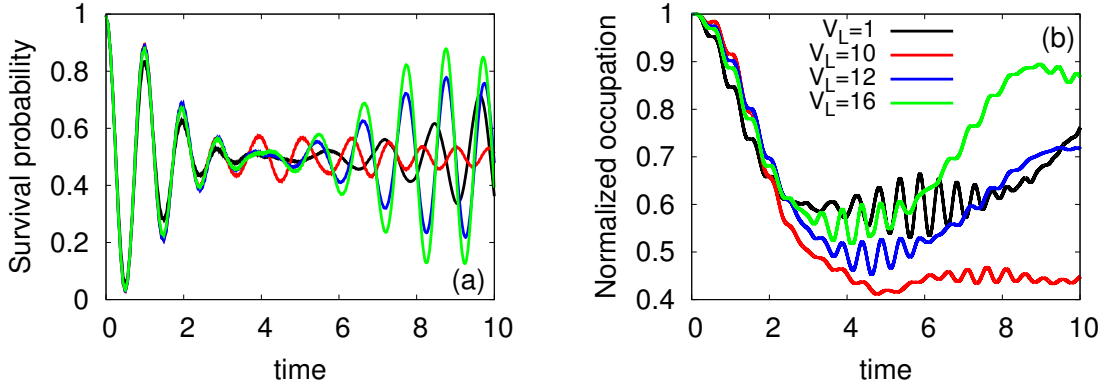


FIG. 4. Tunneling dynamics for stronger interaction. (a) Time-dependent survival probability in the left side of space,  $P(t)$ , and (b) normalized occupation per particle of the ground orbital,  $\eta(t) = n_1(t)/n_1(0)$ . The inter-boson interaction is  $10\Lambda_0$  and the number of bosons  $N = 10$ . Color codes are explained in panel (b). We show here dimensionless quantities.

So far we have dealt with the dynamics of various quantities of a rather weakly interacting system with number of bosons,  $N = 10$ . Now we investigate the interference for a comparatively stronger interaction,  $10\Lambda_0$ , to see whether the rules we have discovered for the tunneling mechanism of fragmented BECs persist for stronger interaction and, moreover, whether there are additional rules. Fig. 4 presents the time evolution of  $P(t)$  and  $\eta(t)$  for the interaction parameter  $10\Lambda_0$ . Here  $P(t)$  exhibits substantial rich physics of the tunneling dynamics of different order of fragmented initial states. First of all, the density never tunnels to 100% for all barrier heights, as the longitudinal fragmentation develops at the very beginning of the tunneling process due to the stronger interaction. Including the density collapse, also found for the weaker interaction, here we observe the different rate of revival of the density oscillations depending on the interference of the initial transversal fragmentation in the system and the developed longitudinal fragmentation in the tunneling process. We find that when the barrier height gradually reaches from  $V_L = 1$  to  $V_L = 10$  the rate of revival of the density oscillations decreases. Further increase of the barrier height, i.e., when  $V_L > 10$ , the revival of the density oscillations increases and reaches its maximal

value when the ground state is initially fully fragmented.

The different rate of the revival process can be explained by the dynamics of  $\eta(t)$ , shown in Fig. 4 (b). The general feature is that all the ground states lose their coherence with an oscillatory background as time progresses. The maximal decay rate of  $\eta(t)$ , found at  $V_L = 10$ , is the result of the maximal interference of the longitudinal and transversal fragmentations, see [45], which is consistent with the rule found for the weaker interaction. Here we also find that the rate of loss of coherence of a fully fragmented BEC, without coupling of the longitudinal and transversal fragmentations, is slower compared to the fully condensed state. Moreover, we find that the rate of revival decreases when one moves from  $V_L = 1$  to  $V_L = 10$ . Further increase of  $V_L$ ,  $\eta(t)$  increases and becomes maximal for  $V_L = 16$ . Therefore, the time-evolution of  $\eta(t)$  for stronger interaction exhibits two new rules for the revival dynamics of fragmented BECs: (i) the interference of the longitudinal and transversal fragmentations opposes the revival process and (ii) a fully fragmented state, without coupling between the longitudinal and transversal fragmentations, speeds up the process of revival.

In conclusion, we explore the Josephson dynamics of complicated bosonic objects which undergoes a rich pathway from condensation to fragmentation in a transversal double-well. We would like to bring out that such intricate ground states shows new rules while tunneling. We have demonstrated the physics behind the tunneling dynamics of the fragmented BEC by emphasizing on the three limiting cases: the first, when the ground state is initially fully condensed, the second, when the interference of the longitudinal and transversal fragmentations is maximal, and the third, when the ground state is initially fully fragmented with no coupling between the fragmentations in the tunneling process. We have established that the interference of the longitudinal and transversal fragmentations opens up a new mechanism of the quantum tunneling process by analyzing the survival probability, details of fragmentation, and transversal position variance in the junction. It is found that the interference of the fragmentations speeds up the density collapse while tunneling and behaves as an opposing force for the revival process. Moreover, the fully fragmented BEC expedites the revival process compared to the fully condensed BEC.

As the four well set-up considered here is a substructure of a two-dimensional optical lattice, tunneling of different quantum phases, such as, superfluid, Mott insulator, [46] and fermionized Tonks–Girardeau gas [47, 48], can be studied by tuning the barrier height and the strength of inter-particle interaction. Moreover, dipolar bosonic crystal orders and the

dynamics of bosons in two-dimensional optical lattice, including the impact of competition of longitudinal and transversal fragmentations, have the future scope to be investigated.

This research was supported by the Israel Science Foundation (Grants No. 447/17 and 1516/19). AB acknowledges Sunayana Dutta for some helpful discussions. Computation time on the High Performance Computing system Hive of the Faculty of Natural Sciences at University of Haifa, and the Hawk at the High Performance Computing Center Stuttgart (HLRS) is gratefully acknowledged.

---

\* [abhowmik@campus.haifa.ac.il](mailto:abhowmik@campus.haifa.ac.il)

- [1] I. Bloch, J. Dalibard, and W. Zwerger, *Rev. Mod. Phys.* **80**, 885 (2008).
- [2] A. Burchinati, C. Fort, and M. Modugno, *Phys. Rev. A* **95**, 023627 (2017).
- [3] S. Levy, E. Lahoud, I. Shomroni, and J. Steinhauer, *Nature (London)* **449**, 579 (2007).
- [4] A. Smerzi, S. Fantoni, S. Giovanazzi, and S. R. Shenoy, *Phys. Rev. Lett.* **79**, 4950 (1997).
- [5] M. Albiez, R. Gati, J. Fölling, S. Hunsmann, M. Cristiani, M. K. Oberthaler, *Phys. Rev. Lett.* **95**, 010402 (2005).
- [6] G. J. Milburn, J. Corney, E. M. Wright, D. F. Walls, *Phys. Rev. A* **55**, 4318 (1997).
- [7] T. Schumm, S. Hofferberth, L. M. Andersson, S. Wildermuth, S. Groth, I. Bar-Joseph, J. Schmiedmayer, and P. Krüger, *Nature Physics* **1**, 57 (2005).
- [8] C. Orzel, A. K. Tuchman, M. L. Fenselau, M. Yasuda, and M. A. Kasevich, *Science* **291**, 2386 (2001).
- [9] Q. Wu, L. Mancino, M. Carlesso, M. A. Ciampini, L. Magrini, N. Kiesel, and M. Paternostro, *PRX Quantum* **3**, 010322 (2022).
- [10] T. Zibold, E. Nicklas, C. Gross, and M. K. Oberthaler, *Phys. Rev. Lett.* **105**, 204101 (2010).
- [11] M. Abbarchi, A. Amo, V. G. Sala, D. D. Solnyshkov, H. Flayac, L. Ferrier, I. Sagnes, E. Galopin, A. Lemaître, G. Malpuech, and J. Bloch, *Nature Physics* **9**, 275 (2013).
- [12] G. Valtolina, A. Burchianti, A. Amico, E. Neri, K. Khani, J. A. Seman, A. Trombettoni, A. Smerzi, M. Zaccanti, M. Inguscio, and G. Roati, *Science* **350**, 1505 (2015).
- [13] J. Hou, X. -W. Luo, K. Sun, T. Bersano, V. Gokhroo, S. Mossman, P. Engels, and C. Zhang, *Phys. Rev. Lett.* **120**, 120401 (2018).
- [14] P. Nozières and D. Saint James, *J. Phys.* **43**, 1133 (1982).

- [15] R. W. Spekkens and J. E. Sipe, Phys. Rev. A **59**, 3868 (1999).
- [16] E. J. Mueller, T. -L. Ho, M. Ueda, and G. Baym Phys. Rev. A **74**, 033612 (2006).
- [17] P. Bader and U. R. Fischer, Phys. Rev. Lett. **103**, 060402 (2009).
- [18] Q. Zhou and X. Cui, Phys. Rev. Lett. **110**, 140407 (2013).
- [19] M. -K. Kang and U. R. Fischer, Phys. Rev. Lett. **113**, 140404 (2014).
- [20] A. U. J. Lode and C. Bruder, Phys. Rev. Lett. **118**, 013603 (2017).
- [21] B. Chatterjee, C. L  v  que, J. Schmiedmayer, and A. U. J. Lode, Phys. Rev. Lett. **125**, 093602 (2020).
- [22] K. Sakmann, A. I. Streltsov, O. E. Alon, and L. S. Cederbaum, Phys. Rev. Lett. **103**, 220601 (2009).
- [23] J. Vargas, M. Nuske, R. Eichberger, C. Hippler, L. Mathey, and A. Hemmerich, Phys. Rev. Lett. **126**, 200402 (2021).
- [24] J. Erdmann, S. I. Mistakidis, and P. Schmelcher, Phys. Rev. A **98**, 053614 (2018).
- [25] F. Theel, K. Keiler, S. I. Mistakidis, and P. Schmelcher, New J. Phys. **22**, 023027 (2020).
- [26] C. Sias, A. Zenesini, H. Lignier, S. Wimberger, D. Ciampini, O. Morsch, and E. Arimondo, Phys. Rev. Lett. **98**, 120403 (2007).
- [27] O. Fialko, A. S. Bradley, and J. Brand, Phys. Rev. Lett. **108**, 015301 (2012).
- [28] G. Spagnolli, G. Semeghini, L. Masi, G. Ferioli, A. Trenkwalder, S. Coop, M. Landini, L. Pezz  , G. Modugno, M. Inguscio, A. Smerzi, and M. Fattori, Phys. Rev. Lett. **118**, 230403 (2017).
- [29] A. Burchianti, F. Scazza, A. Amico, G. Valtolina, J. A. Seman, C. Fort, M. Zaccanti, M. Inguscio, and G. Roati, Phys. Rev. Lett. **120**, 025302 (2018).
- [30] K. Xhani, E. Neri, L. Galantucci, F. Scazza, A. Burchianti, K. -L. Lee, C. F. Barengi, A. Trombettoni, M. Inguscio, M. Zaccanti, G. Roati, and N. P. Proukakis, Phys. Rev. Lett. **124**, 045301 (2020).
- [31] A. Bhowmik and O. E. Alon, Sci. Rep. **12**, 627 (2022).
- [32] J. Christensson, C. Forss  n, S.   berg, S. M. Reimann, Phys. Rev. A **79**, 012707 (2009).
- [33] R. A. Doganov, S. Klaiman, O. E. Alon, A. I. Streltsov, and L. S. Cederbaum, Phys. Rev. A **87**, 033631 (2013).
- [34] U. R. Fischer, A. U. J. Lode, and B. Chatterjee, Phys. Rev. A **91**, 063621 (2015).
- [35] A. I. Streltsov, O. E. Alon, and L. S. Cederbaum Phys. Rev. Lett. **99**, 030402 (2007).

- [36] O. E. Alon, A. I. Streltsov, and L. S. Cederbaum, *Phys. Rev. A* **77**, 033613 (2008).
- [37] J. H. V. Nguyen, M. C. Tsatsos, D. Luo, A. U. J. Lode, G. D. Telles, V. S. Bagnato, and R. G. Hulet, *Phys. Rev. X* **9**, 011052 (2019).
- [38] A. U. J. Lode, C. L  v  que, L. B. Madsen, A. I. Streltsov, and O. E. Alon, *Rev. Mod. Phys.* **92**, 011001 (2020).
- [39] S. Kr  nke, L. Cao, O. Vendrell, and P. Schmelcher, *New J. Phys.* **15**, 063018 (2013).
- [40] L. Cao, S. Kr  nke, O. Vendrell, and P. Schmelcher, *J. Chem. Phys.* **139**, 134103 (2013).
- [41] J. Chen, J. M. Schurer, and P. Schmelcher, *Phys. Rev. Lett.* **121**, 043401 (2018).
- [42] J. M. Schurer, A. Negretti, and P. Schmelcher, *Phys. Rev. Lett.* **119**, 063001 (2017).
- [43] S. I. Mistakidis, G. C. Katsimiga, G. M. Koutentakis, Th. Busch, and P. Schmelcher, *Phys. Rev. Lett.* **122**, 183001 (2019).
- [44] F. Dalfovo, S. Giorgini, L. P. Pitaevskii, and S. Stringari, *Rev. Mod. Phys.* **71**, 463 (1999).
- [45] Supplemental materials of this work.
- [46] M. Capello, F. Becca, M. Fabrizio, and S. Sorella, *Phys. Rev. Lett.* **99**, 056402 (2007).
- [47] V. Dunjko, V. Lorent, and M. Olshanii, *Phys. Rev. Lett.* **86**, 5413 (2001).
- [48] B. Paredes, A. Widera, V. Murg, O. Mandel, S. F  lling, I. Cirac, G. V. Shlyapnikov, T. W. H  nsch, and I. Bloch, *Nature (London)* **429** 277 (2004).

## SUPPLEMENTAL MATERIAL: INTERFERENCE OF LONGITUDINAL AND TRANSVERSAL FRAGMENTATIONS IN THE JOSEPHSON DYNAMICS OF BOSE-EINSTEIN CONDENSATES

In this supplemental material, we promote the main text with further details. Here we start with a brief mathematical description on the many-particle variance discussed in the main text. Moving forward, to represent and compare Josephson dynamics of different fragmented states, we require a fixed time scale. Therefore, we present the longitudinal and transversal Rabi frequencies in the four well set up, considered in the main text, as a function of  $V_L$ . Further, as a basic analysis tool of the Josephson dynamics presented here, we provide the mean-field results of the dynamics of the survival probability, and the longitudinal and transversal position variances. Moreover, in order to go deeper to the understanding of the interference in different fragmentation channels, we demonstrate the details of the fragmentation processes in terms of the occupancy of the higher natural orbitals and their connection with many-body longitudinal and transversal position variances. Next, we discuss the robustness of our results on the width of the inter-boson interaction potential. Finally, we present the convergences of our results.

### MANY-PARTICLE POSITION VARIANCE

The main text contains the results of the many-particle position variance which determines how the interference of the longitudinal and transversal fragmentations develops during the tunneling process. Here we present the mathematical formula of the many-particle position variance. The time-dependent variance per particle of an operator,  $\hat{A}$ , is determined by the combination of the expectation values of  $\hat{A}$  and  $\hat{A}^2$ . The expectation value of  $\hat{A} = \sum_{j=1}^N \hat{a}(r_j)$  depends only on the one-body operators. Also the value of  $\hat{A}^2$  is  $\hat{A}^2 = \sum_{j=1}^N \hat{a}^2(r_j) + \sum_{j < k} 2\hat{a}(r_j)\hat{a}(r_k)$ . Consequently, the variance is expressed as [?] ]

$$\begin{aligned}
\frac{1}{N}\Delta_A^2(t) &= \frac{1}{N}[\langle\Psi(t)|\hat{A}^2|\Psi(t)\rangle - \langle\Psi(t)|\hat{A}|\Psi(t)\rangle^2] \\
&= \frac{1}{N}\left\{ \sum_j n_j(t) \int d\mathbf{r} \phi_j^*(\mathbf{r}; t) \hat{a}^2(\mathbf{r}) \phi_j(\mathbf{r}; t) - \left[ \sum_j n_j(t) \int d\mathbf{r} \phi_j^*(\mathbf{r}; t) \hat{a}(\mathbf{r}) \phi_j(\mathbf{r}; t) \right]^2 \right. \\
&\quad \left. + \sum_{jpkq} \rho_{jpkq}(t) \left[ \int d\mathbf{r} \phi_j^*(\mathbf{r}; t) \hat{a}(\mathbf{r}) \phi_k(\mathbf{r}; t) \right] \left[ \int d\mathbf{r} \phi_p^*(\mathbf{r}; t) \hat{a}(\mathbf{r}) \phi_q(\mathbf{r}; t) \right] \right\}, \quad (0.2)
\end{aligned}$$

where  $\{\phi_j(\mathbf{r}; t)\}$  are the natural orbitals,  $\{n_j(t)\}$  the natural occupations, and  $\rho_{jpkq}(t)$  are the elements of the reduced two-particle density matrix,  $\rho(\mathbf{r}_1, \mathbf{r}_2, \mathbf{r}'_1, \mathbf{r}'_2; t) = \sum_{jpkq} \rho_{jpkq}(t) \phi_j^*(\mathbf{r}'_1; t) \phi_p^*(\mathbf{r}'_2; t) \phi_k(\mathbf{r}_1; t) \phi_q(\mathbf{r}_2; t)$ . For one-body operators which are local in position space, the variance described in Eq 0.2 reduces to [2]

$$\frac{1}{N}\Delta_A^2(t) = \int d\mathbf{r} \frac{\rho(\mathbf{r}; t)}{N} \hat{a}^2(\mathbf{r}) - N \left[ \int \frac{\rho(\mathbf{r}; t)}{N} \hat{a}(\mathbf{r}) \right]^2 + \int d\mathbf{r}_1 d\mathbf{r}_2 \frac{\rho^{(2)}(\mathbf{r}_1, \mathbf{r}_2, \mathbf{r}_1, \mathbf{r}_2; t)}{N} \hat{a}(\mathbf{r}_1) \hat{a}(\mathbf{r}_2). \quad (0.3)$$

## LONGITUDINAL AND TRANSVERSAL RABI FREQUENCIES FOR THE FOUR-WELL SET-UP

The tunneling of bosons, demonstrated in the main text, occurs for various barrier heights,  $V_L$ . Therefore, to compare our results, a natural choice of time scale is required. Fig. S1 provides the Rabi frequencies (in logarithmic scale) as a function of barrier height along the longitudinal and transversal directions,  $t_{Rabi} = \frac{2\pi}{E_X - E_0}$  and  $t'_{Rabi} = \frac{2\pi}{E_Y - E_0}$ , respectively, where  $E_0$  is the energy of the ground state, and  $E_X$  and  $E_Y$  represent the energies of the first excited states along the  $x$ - and  $y$ -directions, respectively. Here, the Rabi frequencies are calculated by diagonalizing the single-particle Hamiltonian using the discrete variable representation method. The trapping potential described in the main text, with the increasing barrier height, changes from a double-well to a four-well potential. As the one-body Hamiltonian is separable, it is noticed that  $t_{Rabi}$  does not change with the barrier height with value 132.498 whereas  $t'_{Rabi}$  monotonously grows.  $t'_{Rabi}$  crosses  $t_{Rabi}$  when  $E_Y \approx E_X$  at  $V_L = 8$ . As we are interested in the tunneling dynamics along the longitudinal direction, we set the time-scale of the dynamics as  $t/t_{Rabi}$ .

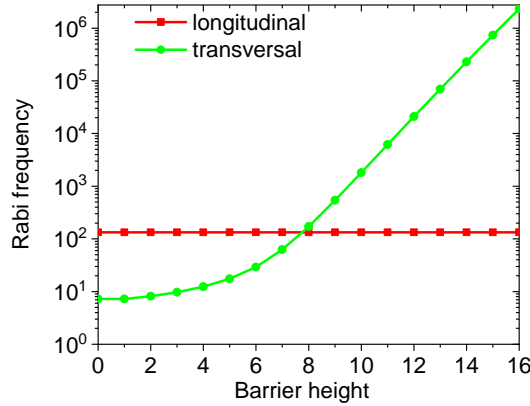


FIG. S1. Rabi frequencies (in logarithmic scale) along the longitudinal and transversal directions are presented as a function of barrier height,  $V_L$ , using the trapping potential described in dynamics of the main text. We show here dimensionless quantities.

### MEAN-FIELD SURVIVAL PROBABILITY

We have seen in the main text that the amplitude of the many-body survival probability,  $P(t)$ , decays for all barrier heights due to development of the longitudinal fragmentation. Here we show the dynamics of  $P(t)$  as if we would have investigated the tunneling phenomenon under mean-field theory. Fig. S2 depicts the survival probability in the left side of space for the inter-particle interactions  $\Lambda_0$  and  $10\Lambda_0$ . Here, in the mean-field dynamics, we observe that 100% of the particles tunnel back and forth between the left and right parts of space with practically the same frequency of oscillations as a function of the barrier height. Therefore, Fig. S2 exhibits that the mean-field survival probability essentially does not depend on the shape of the initial density structure of the ground states, barrier height, and the considered inter-bosons interaction strengths. This is in sharp distinction from the many-body dynamics.

### DETAILS OF THE MANY-BODY FRAGMENTATIONS

The main text shows that the occupation of the first natural orbital decreases with time which signifies the growing occupations of the higher natural orbitals. Now, we examine and compare the microscopic mechanism of how the higher natural orbitals,  $\frac{n_{j=2,3,4}(t)}{N}$ , become



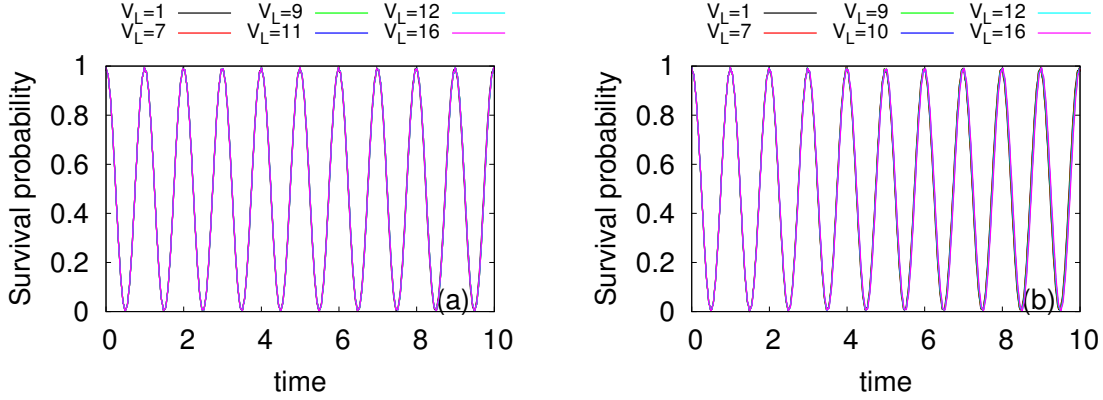


FIG. S2. Time-dependent mean-field survival probability in the left side of space,  $P(t)$ , for the interaction strengths (a)  $\Lambda_0$  and (b)  $10\Lambda_0$ . We show here dimensionless quantities.

populated as a function of  $V_L$ . Figs. S3 and S4 depict the occupations of the most dominant higher natural orbitals, i.e., the second, third, and fourth natural orbitals for the interaction strengths  $\Lambda_0$  and  $10\Lambda_0$ , respectively.

Let us start with the discussion of Fig. S3. If one gradually moves from  $V_L = 1$  to 7, the initial state continuously deforms yet maintaining its coherency. The deformation of the initial ground state delays the process of losing the coherence in the dynamics. Therefore, from  $V_L = 1$  to  $V_L = 7$ , although all the higher natural orbitals become occupied with time, the rate of occupancy of the second natural orbital is faster for  $V_L = 1$  compared to  $V_L = 7$ . From  $V_L = 1$  to 7, the second, third, and fourth natural orbitals are excited  $g$ -, and  $u$ -, and excited  $u$ -orbitals, respectively, discussed in the main text. The order of populations of the orbitals is preserved throughout the dynamics until  $V_L = 7$ , i.e., excited  $g$ -orbital >  $u$ -orbital > excited  $u$ -orbital.

Remarkably, at the beginning of the dynamics found at  $V_L \geq 8$ , the second natural orbital loses its coherence along with the first natural orbital. Here, the second, third, and fourth natural orbitals are  $u$ -, excited  $g$ -, and excited  $u$ -orbitals, respectively. The loss of coherence of the  $u$ -orbital occurs due to its sufficient initial occupation at  $V_L \geq 8$  and it mimics the trends of the  $g$ -orbital. This loss of coherence of the  $u$ -orbital is a purely many-body phenomenon and occurs only for the fragmented ground state. If the ground state is initially more fragmented, depending on the barrier height, the  $u$ -orbital follows the trend of loss of coherence for longer times in the process of tunneling. The  $u$ -orbital loses its coherence until the time when there is a swapping of orders of populations between two higher natural

orbitals. At  $V_L = 9$  and 10, we observe that the  $u$ - and excited  $g$ -orbitals exchange their orders at  $t = 0.76$  and 2.11, respectively, and afterwards, the  $u$ -orbital builds up coherence, see the insets of Figs. S3 (c) and (d). This build up of coherence in the  $u$ -orbital reflects the interference of the longitudinal and transversal fragmentations.

At  $V_L = 11$ , the microscopic mechanism of the fragmentation becomes more richer. Here we find that the build up of coherence in the  $u$ -orbital is accompanied by the swapping of orders of populations of excited  $g$ - and excited  $u$ -orbitals at  $t = 4.56$ . Further, around  $t = 17$ , the  $u$ - and excited  $u$ -orbitals exchange their orders three times and afterwards, the  $u$ -orbital builds up coherence. At  $V_L = 12$ , the build up of coherence in the  $u$ -orbital occurs when the excited  $g$ - and excited  $u$ -orbitals swap their orders. Also, similar to the fragmentation mechanism found at  $V_L = 9$  and 10, the build up of coherence in the  $u$ -orbital is accompanied by a swapping of the orders of the  $u$ - and excited  $g$ -orbitals.

At  $V_L = 16$ , as the initial state is almost fully fragmented and there is almost no coupling between the longitudinal and transversal fragmentations, the  $u$ -orbital retains the trends of loss of coherence. Accordingly, the populations of the excited  $g$ - and excited  $u$ -orbitals monotonously grow. All in all, the interference of the longitudinal and transversal fragmentations manifests in the build up of coherence in the  $u$ -orbital and we find that the interference is maximal at  $V_L = 12$  for the considered inter-boson interaction  $\Lambda_0$ .

Now we discuss the time-evolution of  $\frac{n_{j=2,3,4}(t)}{N}$  for the stronger inter-boson interaction  $10\Lambda_0$ , see Fig. S4, and find how it leads to a qualitatively different microscopic mechanism of fragmentation found for the weaker interaction  $\Lambda_0$ . We observed, for the weaker interaction, that whenever the  $u$ -orbital breaks its natural trend from loss of coherence to build up of coherence, the  $u$ - and excited  $g$ - or the excited  $g$ - and excited  $u$ -orbitals interchange their orders. Here, for  $10\Lambda_0$ , we find that the orders of the orbitals interchange multiple times, for example see for  $V_L = 10$  and  $V_L = 12$ . Although at the smaller barrier height, say at  $V_L = 9$ , the  $u$ - and excited  $g$ -orbitals exchange their orders only once. For  $V_L = 10$ , the  $u$ -orbital breaks its trend twice from loss of coherence to build up of coherence, at  $t = 0.66t_{Rabi}$  and  $3.60t_{Rabi}$ . For the former time, the excited  $g$ - and excited  $u$ -, and for the latter time, the  $u$ - and excited  $u$ -orbitals interchange their orders. Remarkably, at  $V_L = 12$ , the  $u$ - and excited  $g$ -orbitals interchange their orders twelve times between  $t = 3t_{Rabi}$  and  $6t_{Rabi}$ . Therefore, for strong interaction, we observe that the  $u$ -orbital breaks its trends of loss of coherence to build up of coherence multiple times due to the interchange of order of either the  $u$ - and

excited  $g$ - or the excited  $g$ - and excited  $u$ - or the  $u$ - and excited  $u$ -orbitals. Here we find that the transition from loss of coherence to build up of coherence or vice versa is always accompanied by the interchange of orders of higher natural orbitals until revival takes place. In the two extreme barrier heights considered, at  $V_L = 1$ , the  $u$ -orbital shows transition from build up of coherence to loss of coherence and, at  $V_L = 16$ , from loss of coherence to build up of coherence, due to the pure effect of revival process.

Now, we determine at which barrier height the interference of longitudinal and transversal fragmentations is maximal for the inter-boson interaction  $10\Lambda_0$ , see Fig. S5. The interference is calculated from the difference between maximal occupancy of the  $u$ -orbital after building up of coherence (but before the revival process) and its initial occupancy. We find that at the intermediate barrier heights, from  $V_L = 8$  to  $V_L = 12$ , the interference of longitudinal and transversal fragmentations take place and, for  $10\Lambda_0$ , the maximal interference occurs at  $V_L = 10$ . Therefore, with the increase of inter-boson interaction, the maximal interference appears at the lower barrier height, compare to Fig. 2(c) of the main text.

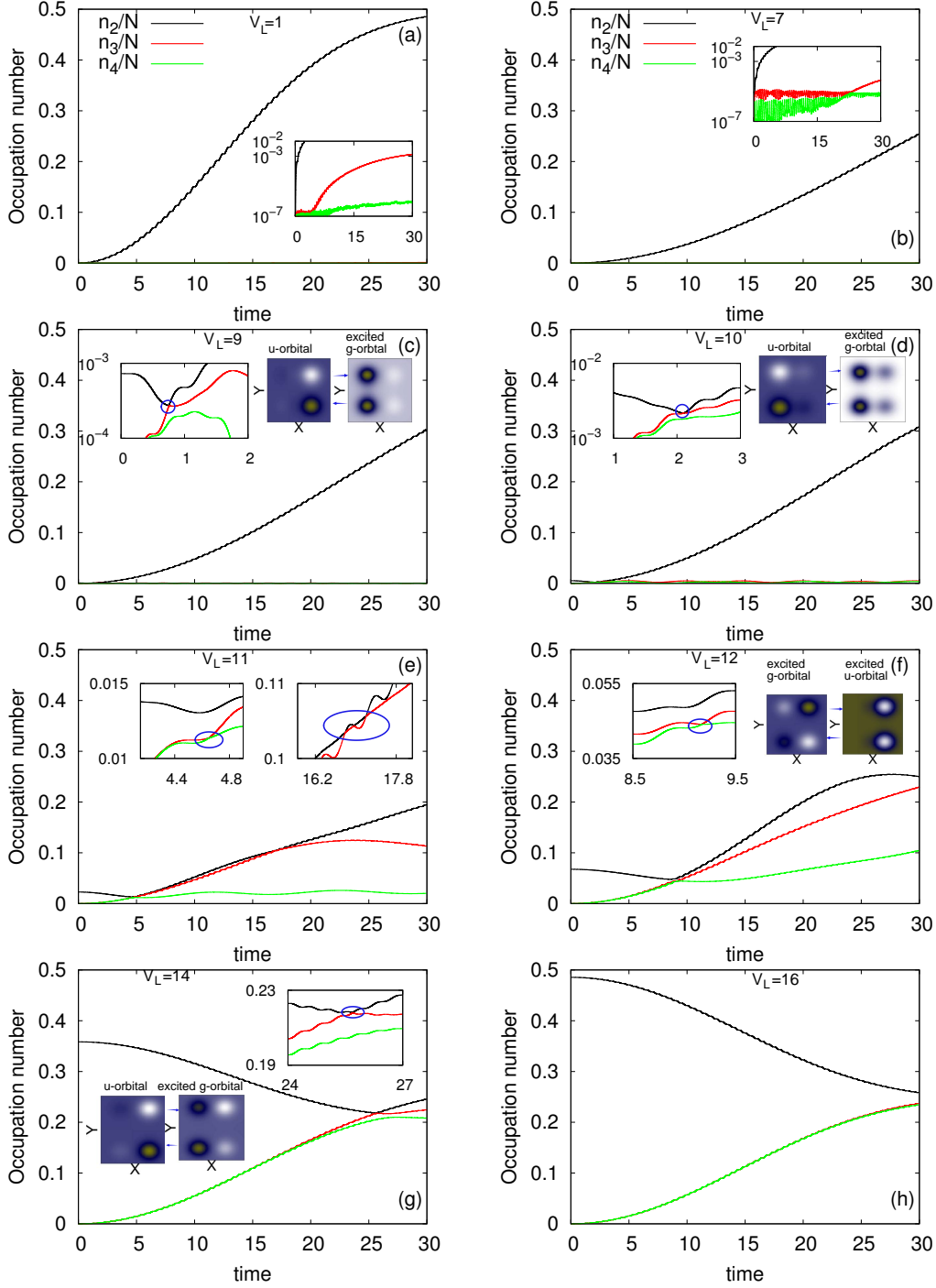


FIG. S3. Details of the fragmentations. Time evolution of the occupation numbers per particle of the higher natural orbitals,  $\frac{n_{j=2,3,4}(t)}{N}$ , for different barrier heights. The inter-boson interaction is  $\Lambda_0$  and the number of bosons  $N = 10$ . The insets of panels (a) to (g) magnify the same plots. In the insets of panels (c), (d), (f), and (g), we also present swapping of orders of the orbitals. This swapping of orbitals happens when the  $u$ -orbital shows a transition from loss of coherence to build up of coherence. To guide the eye, we mark the time of swapping of orders of the orbitals with a blue circle. Color codes are explained in panels (a) and (b). We show here dimensionless quantities.

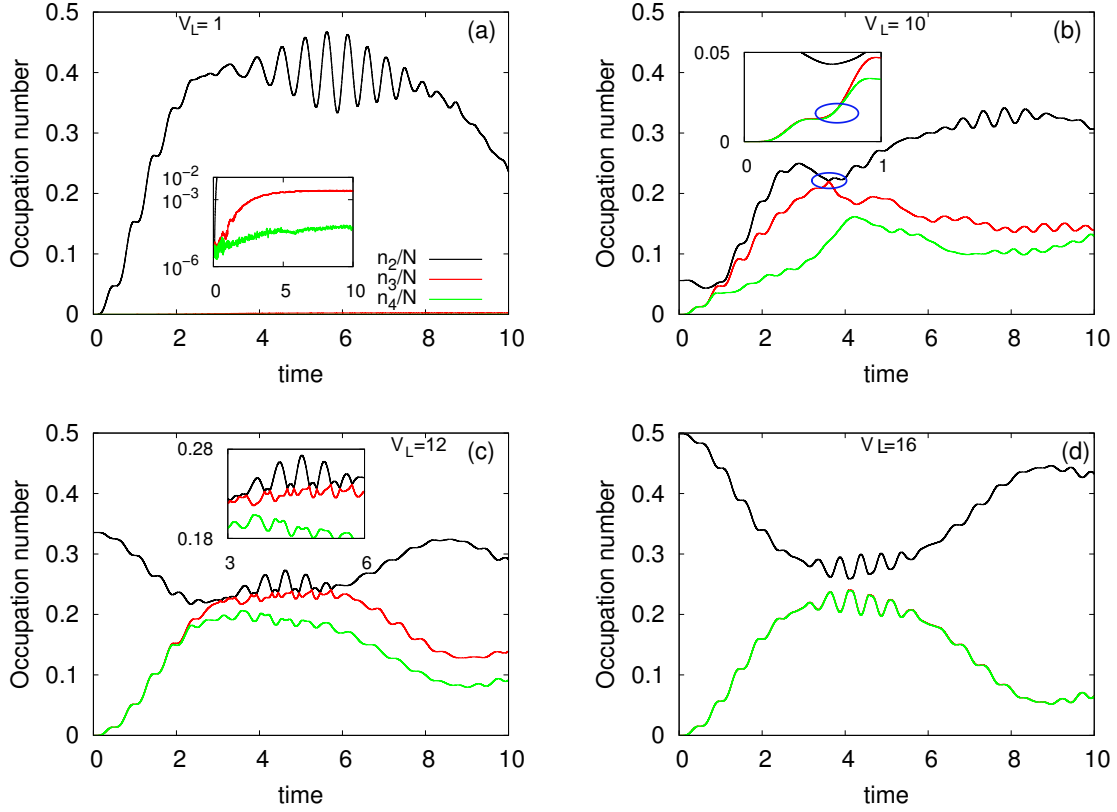


FIG. S4. Details of the fragmentations. Time evolution of the occupation numbers per particle of the higher natural orbitals,  $\frac{n_{j=2,3,4}(t)}{N}$ , for different barrier heights. The inter-boson interaction is  $10\Lambda_0$  and the number of bosons  $N = 10$ . The insets of panels (a) to (c) magnify the same plots. In the inset of panel (b), we present swapping of orders of the orbitals. This swapping of orders happens when the  $u$ -orbital shows a transition from loss of coherence to build up of coherence. To guide the eye, we mark the time of swapping of orbitals with a blue circle. Color codes are explained in panel (a). We show here dimensionless quantities.

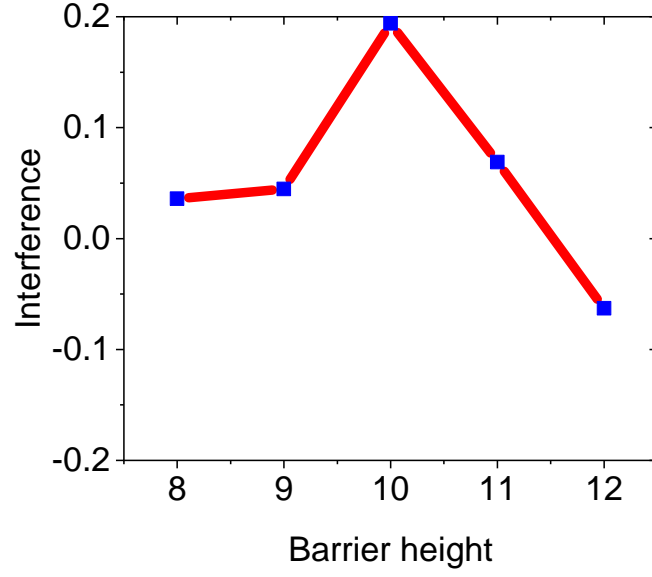


FIG. S5. Interference of longitudinal and transversal fragmentations. The interference is determined from the difference between maximal occupancy of the  $u$ -orbital after build up of coherence and its initial occupancy. occupation numbers per particle of the higher natural. The inter-boson interaction is  $10\Lambda_0$  and the number of bosons  $N = 10$ . We show here dimensionless quantities.

## DYNAMICS OF LONGITUDINAL AND TRANSVERSAL POSITION VARIANCES

Here we start our discussion with the position variance to analyze: (i) how ground states of different shapes tunnel when the fragmentation is not accounted in the system and (ii) the Josephson tunneling dynamics in the mean-field limit. Fig. S6 records the mean-field longitudinal and transversal position variances,  $\frac{1}{N}\Delta_X^2(t)$  and  $\frac{1}{N}\Delta_Y^2(t)$ , respectively, for the inter-particle interaction  $\Lambda_0$ . Fig. S6 (a) shows that the mean-field dynamics of  $\frac{1}{N}\Delta_X^2(t)$  is practically independent of the barrier height,  $V_L$ . Whereas the mean-field  $\frac{1}{N}\Delta_X^2(t)$  essentially does not depend on the barrier height for the time durations considered here,  $\frac{1}{N}\Delta_Y^2(t)$  monotonously increases with  $V_L$  having almost a frozen dynamical behavior (fluctuation around  $10^{-3}$ ). This monotonous increase of the base value of  $\frac{1}{N}\Delta_Y^2(t)$  is originated due to the initial deformation in the ground state. For the increased interaction strength  $10\Lambda_0$ , we find that  $\frac{1}{N}\Delta_X^2(t)$  shows practically the same dynamical behavior found for  $\Lambda_0$ . Also now,  $\frac{1}{N}\Delta_Y^2(t)$  shows an essentially frozen dynamics for  $10\Lambda_0$ , but the base values are different for the intermediate barrier heights  $V_L = 7$  to  $V_L = 14$  in comparison to those found for  $\Lambda_0$ . The different base values are evident from the initial values of  $\frac{1}{N}\Delta_Y^2(t)$ , see Fig. 1(b) of the main text. Therefore, it suggests that the regime of the inter-boson interaction strength considered in this work does not have any qualitative impact on the mean-field dynamics of the longitudinal and transversal position variances.

As the main text demonstrates the dynamics of the many-body transversal position variance for the interaction strength  $\Lambda_0$ , here we discuss the impact of the interference of longitudinal and transversal fragmentations on the many-body dynamics of the longitudinal position variance,  $\frac{1}{N}\Delta_X^2(t)$ , see Fig. S7. As a general feature, we find that the many-body  $\frac{1}{N}\Delta_X^2(t)$  oscillates with a growing amplitude and the rate of growth varies depending on  $V_L$ . In comparison with the corresponding mean-field dynamics, the maximal deviation of the many-body  $\frac{1}{N}\Delta_X^2(t)$  occurs at  $V_L = 1$  and the minimal at  $V_L = 12$ . We find that the growth of the many-body  $\frac{1}{N}\Delta_X^2(t)$  maintains its order from  $V_L = 1$  to  $V_L = 10$  which is consistent with the many-body  $P(t)$  and the dynamics of the normalized occupation number,  $\eta(t)$ , discussed in the main text. For example, if we consider the barrier height until  $V_L = 10$ , the many-body  $\frac{1}{N}\Delta_X^2(t)$  shows maximal deviation at  $V_L = 7$  and minimal at  $V_L = 10$  com-

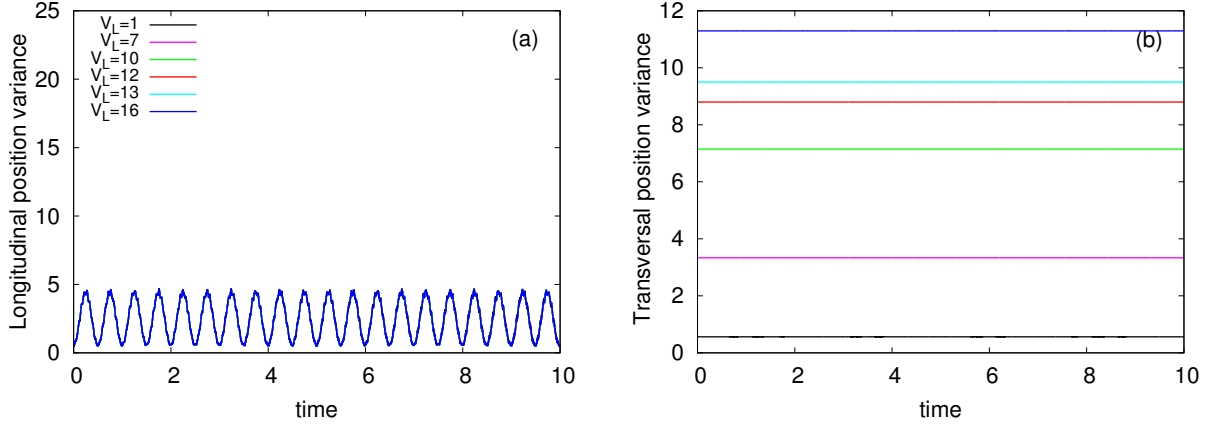


FIG. S6. Time-dependent many-particle position variances per particle along the longitudinal and transversal directions,  $\frac{1}{N}\Delta_X^2(t)$  and  $\frac{1}{N}\Delta_Y^2(t)$ , respectively, for different barrier heights. The inter-boson interaction is  $\Lambda_0$ . The results are obtained by applying the mean-field theory. The results for  $10\Lambda_0$  essentially overlap those for  $\Lambda_0$  and are not plotted. Color codes are explained in the left panel. We show here dimensionless quantities.

pared to the respective many-body dynamics at  $V_L = 1$ , which is consistent with  $P(t)$  and the normalized occupation number. By examining Fig. S7, we notice that the saturation value of the many-body  $\frac{1}{N}\Delta_X^2(t)$  is almost double for the fully condensed state (at  $V_L = 1$ ) compared to the corresponding saturation value for the fully fragmented state (at  $V_L = 16$ ). Moreover, the saturation value of the many-body  $\frac{1}{N}\Delta_X^2(t)$  is minimal when the interference of the longitudinal and transversal fragmentations is maximal. Therefore, by analysing the many-body  $\frac{1}{N}\Delta_X^2(t)$  and  $\frac{1}{N}\Delta_Y^2(t)$  (in the main text), we observe that the interference of the longitudinal and transversal fragmentations hinders in achieving higher saturation value for  $\frac{1}{N}\Delta_X^2(t)$  and helps to increase the amplitude of oscillations of  $\frac{1}{N}\Delta_Y^2(t)$ .

Now we would demonstrate the many-body longitudinal and transversal position variances for the interaction strength  $10\Lambda_0$ , see Fig. S8 (a) and (b), respectively, and provide a further connection with the respective many-body survival probability,  $P(t)$ , and normalized loss of coherence,  $\eta(t)$ , discussed in the main text. From Fig. S8 (a), we find that the many-body dynamics of  $\frac{1}{N}\Delta_X^2(t)$  gradually increases in an oscillatory manner due to the development of longitudinal fragmentation and eventually saturates when the revival takes place. The saturation value of  $\frac{1}{N}\Delta_X^2(t)$  is maximal for  $V_L = 1$ , when the initial state is fully condensed, and minimal for  $V_L = 10$  when the interference of the longitudinal and transversal fragmentations is maximal. The signature of revival shown in the many-body dynamics



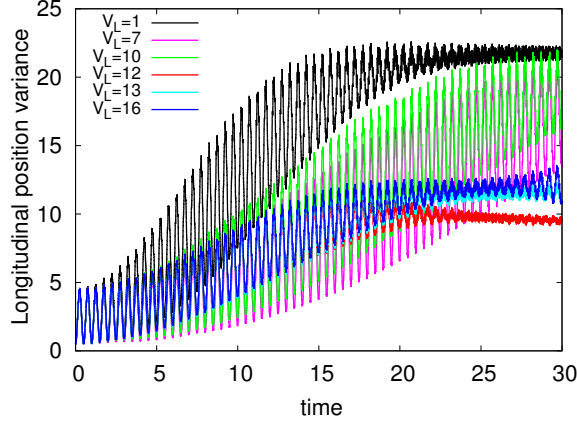


FIG. S7. Time-dependent many-body longitudinal position variance per particle,  $\frac{1}{N}\Delta_{\hat{X}}^2(t)$ , for different barrier heights. The inter-boson interaction is  $\Lambda_0$  and the number of bosons  $N = 10$ . We show here dimensionless quantities.

of  $\frac{1}{N}\Delta_{\hat{X}}^2(t)$  complements the time-evolution of the many-body  $P(t)$  and normalized loss of coherence,  $\eta(t)$ . It is found that the revival in the many-body dynamics of  $\frac{1}{N}\Delta_{\hat{X}}^2(t)$  takes place faster when the system is initially fully fragmented and there is essentially no coupling between the longitudinal and transversal fragmentations in the process of tunneling, i.e., at  $V_L = 16$ . Moreover, the process of revival is delayed when the initial state is transversely fragmented before it starts to couple with the longitudinal fragmentation in the tunneling dynamics.

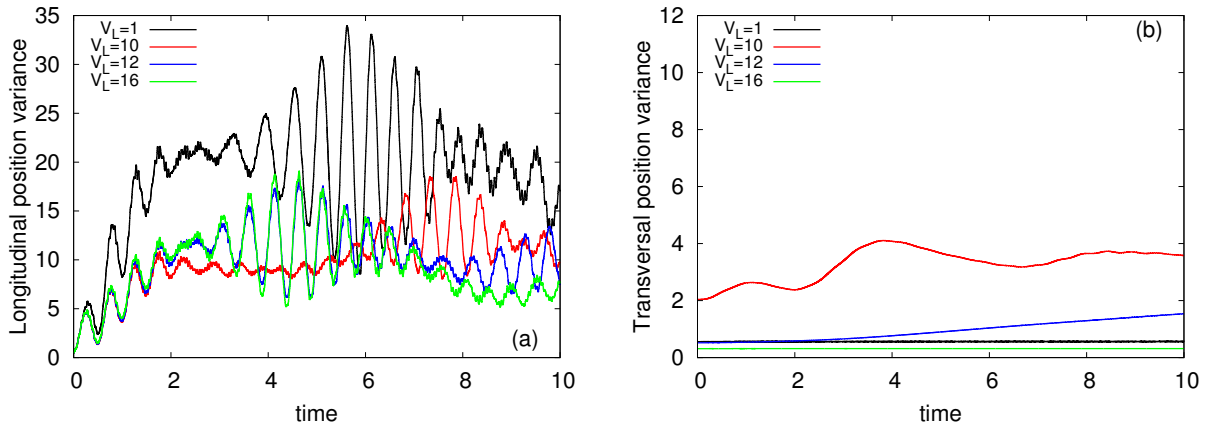


FIG. S8. Time-dependent many-body position variances per particle along the longitudinal and transversal directions,  $\frac{1}{N}\Delta_{\hat{X}}^2(t)$  and  $\frac{1}{N}\Delta_{\hat{Y}}^2(t)$ , respectively, for different barrier heights. The inter-boson interaction is  $10\Lambda_0$  and the number of bosons  $N = 10$ . We show here dimensionless quantities.

Fig. S8 (b) records the many-body dynamics of  $\frac{1}{N}\Delta_Y^2(t)$ . For the lowest barrier height  $V_L = 1$ , when the initial ground state is fully condensed, the dynamics of  $\frac{1}{N}\Delta_Y^2(t)$  is found to be practically frozen as the system is fully condensed. As the interference of the longitudinal and transversal fragmentations takes place, we observe oscillatory nature in the dynamics of  $\frac{1}{N}\Delta_Y^2(t)$ , see for  $V_L = 10$ . Compared to the weak inter-boson interaction, here we find that the period of oscillations of  $\frac{1}{N}\Delta_Y^2(t)$  changes with time due to the combined effect of transversal tunneling and breathing-motion frequencies. The maximal fluctuations of  $\frac{1}{N}\Delta_Y^2(t)$  with a growing amplitude is observed at  $V_L = 10$  which goes hand in hand with the maximal coupling of the longitudinal and transversal fragmentations. As we increase the barrier height  $V_L > 10$ , the interference of the longitudinal and transversal fragmentations gradually becomes smaller and the oscillations of  $\frac{1}{N}\Delta_Y^2(t)$  slowly decay. Eventually, at  $V_L = 16$ , we observe essentially constant dynamical behavior due to the practically null interference of the longitudinal and transversal fragmentations. Therefore, we conclude that the detailed investigation of the many-body dynamics of  $\frac{1}{N}\Delta_Y^2(t)$ , being a sensitive probe of correlations, encodes the interference of longitudinal and transversal fragmentations.

## ROBUSTNESS OF THE RESULTS ON THE WIDTH OF INTER-BOSON INTERACTION POTENTIAL

In the main text, we have made a detailed investigation on the physics of interference of the longitudinal and transversal fragmentations in the tunneling process in two spatial dimensions. For our study, we have used for the inter-boson interaction a Gaussian model potential of finite width,  $\sigma = 0.25\sqrt{\pi}$ . In order to demonstrate the robustness of our results, we recomputed all the properties discussed in this work for two additional smaller widths,  $\sigma = 0.25$  and  $\sigma = 0.25/\sqrt{\pi}$ . Note that we purposely do not use the delta-function to model the inter-boson interaction as the delta-function in two-dimensions does not scatter.

Here, we begin with the discussion of static properties, i.e, the loss of coherence and transversal position variance as a function of the longitudinal barrier height for the widths of the Gaussian model potential  $\sigma = 0.25\sqrt{\pi}$ ,  $0.25$ , and  $0.25/\sqrt{\pi}$ , see Fig. S9. We find that the qualitative physics of the static properties, presented in this work, does not depend on  $\sigma$ . Moreover, the difference between the results, found for  $\sigma = 0.25$  and  $0.25/\sqrt{\pi}$ , is smaller

compared to the respective difference obtained for  $\sigma = 0.25\sqrt{\pi}$  and 0.25. This indicates that decreasing of the width,  $\sigma$ , slowly reduces the quantitative difference of a particular quantity.

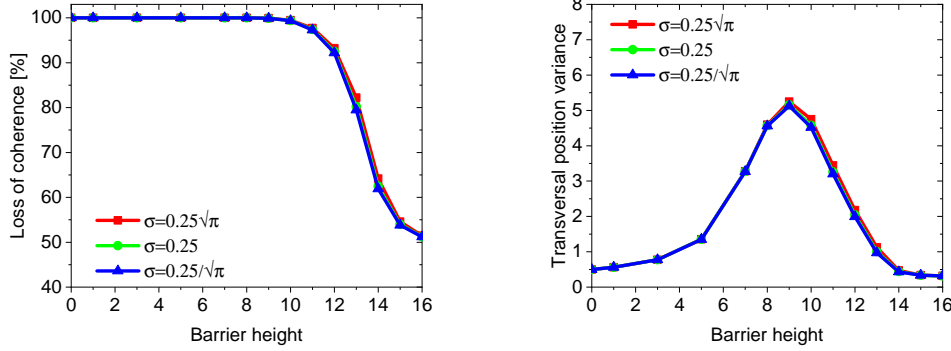


FIG. S9. (a) Loss of coherence and (b) transversal position variance,  $\frac{1}{N}\Delta_Y^2(t)$ , for the three different widths of inter-boson interaction potential, i.e.,  $\sigma = 0.25\sqrt{\pi}$ , 0.25, and  $0.25/\sqrt{\pi}$ , as a function of the longitudinal barrier height ( $V_L$ ). The inter-boson interaction is  $\Lambda_0$  and the number of bosons  $N = 10$ . We show here dimensionless quantities.

To present the robustness of the width,  $\sigma$ , at the many-body dynamics, we select the dynamics of the ground state at  $V_L = 12$  when the interference of the longitudinal and transversal fragmentations is maximal. Fig. S10 depicts the many-body dynamics of loss of coherence,  $\frac{n_1(t)}{N}$ , occupations of the second and third natural orbitals,  $\frac{n_2(t)}{N}$  and  $\frac{n_3(t)}{N}$ , respectively, longitudinal position variance,  $\frac{1}{N}\Delta_X^2(t)$ , and transversal position variance,  $\frac{1}{N}\Delta_Y^2(t)$ , at  $V_L = 12$  for the widths  $\sigma = 0.25\sqrt{\pi}$ , 0.25, and  $0.25/\sqrt{\pi}$ . It is found that  $\frac{n_1(t)}{N}$  is the  $g$ -orbital throughout the tunneling process for all  $\sigma$ . Also, we observe that the  $g$ -orbital loses coherence comparatively quicker (slower) for  $\sigma = 0.25/\sqrt{\pi}$  ( $\sigma = 0.25\sqrt{\pi}$ ) which implies faster (slower) development of fragmentation as shown in Fig. S10 (a). The unchanged qualitative feature of the occupancy of  $g$ -orbital indicates its robustness with the width of inter-boson interaction.

Fig. S10 (b) presents the occupation of the second and third natural orbitals. For  $\sigma = 0.25\sqrt{\pi}$ , discussed in the main text, the second and third natural orbitals remain as  $u$ - and excited  $g$ -orbitals, and the build up of coherence in the  $u$ -orbital manifests the interference of longitudinal and transversal fragmentations. Here, also for the widths  $\sigma = 0.25$  and

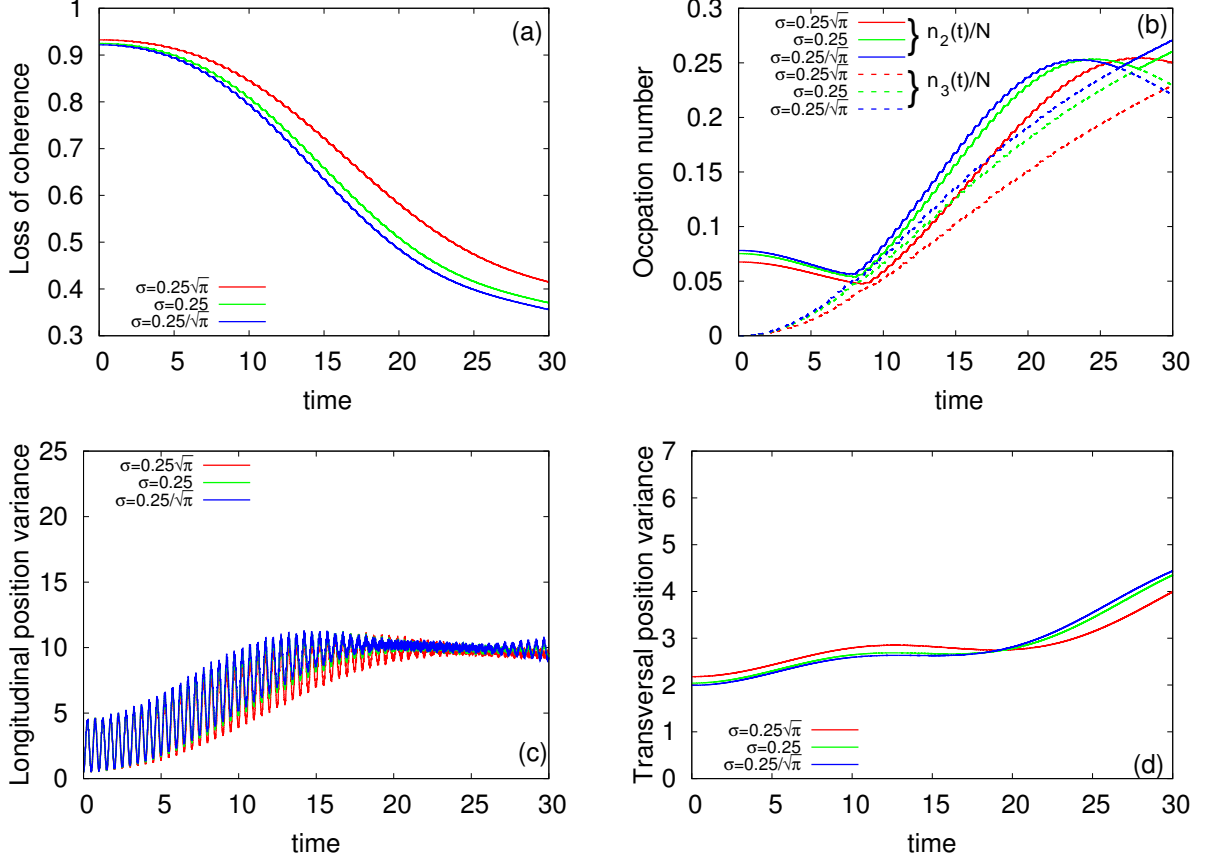


FIG. S10. Dependency of the many-body dynamics of ground state at the barrier height  $V_L = 12$ , for the three different widths of inter-boson interaction potential, i.e.,  $\sigma = 0.25\sqrt{\pi}$ ,  $\sigma = 0.25$ , and  $\sigma = 0.25/\sqrt{\pi}$ . The dynamics is presented by (a) loss of coherence, (b) occupation of the second and third natural orbitals, (c) longitudinal position variance, and (d) transversal position variance. The inter-boson interaction is  $\Lambda_0$  and the number of bosons  $N = 10$ . In panel (b), the solid and dashed lines represent the occupation of the second,  $n_2(t)/N$ , and third,  $n_3(t)/N$ , natural orbitals, respectively. We show here dimensionless quantities.

$0.25/\sqrt{\pi}$ , we observe a build up of coherence in the  $u$ -orbital with the faster rate for the width  $\sigma = 0.25/\sqrt{\pi}$ . It is found that the qualitative features of occupations of the second and third natural orbitals are same for all  $\sigma$  until a swapping between the orders of  $u$ - and excited  $g$ -orbitals happen for  $\sigma = 0.25$  and  $0.25/\sqrt{\pi}$ . This swapping of orders of the orbitals would also happen for  $\sigma = 0.25\sqrt{\pi}$  if one would compute the dynamics for longer time. Therefore, Fig. S10 (b) exhibits the robustness of the interference of longitudinal and transversal fragmentations.

As the variances are the sensitive probe of correlations, we find here that the developed

fragmentation in the system only quantitatively influences the many-body  $\frac{1}{N}\Delta_{\hat{X}}^2(t)$  and  $\frac{1}{N}\Delta_{\hat{Y}}^2(t)$ . Also, Figs. S10 (c) and (d) attribute that decreasing the width of the inter-boson interaction potential gradually diminishes the quantitative difference between the dynamics of a given quantity. All in all, we observe that the width of the inter-boson interaction potential does not qualitatively impact the many-body physics of the interference of fragmentations focused and discussed in this work.

Further, we have computed all the quantities at all barrier heights for the inter-boson interaction strength  $10\Lambda_0$  with the two additional smaller widths,  $\sigma = 0.25$  and  $0.25/\sqrt{\pi}$ . We have checked that the qualitative physics of the dynamics of the different orders of fragmented states is independent of  $\sigma$  for the stronger interaction  $10\Lambda_0$  and thus are not shown graphically.

Finally, in the mean-field dynamics, we notice that the time-evolution of all the quantities obtained for  $\sigma = 0.25$  and  $\sigma = 0.25/\sqrt{\pi}$  fall on top of the respective results computed for  $\sigma = 0.25\sqrt{\pi}$  (not shown). Therefore, the width of the inter-boson interaction does essentially not influence the mean-field dynamics presented in this work, which is interesting for itself.

## DETAILS OF CONVERGENCES OF QUANTITIES IN THE TUNNELING DYNAMICS

The multiconfigurational time-dependent Hartree for bosons (MCTDHB) method is used in the present work to compute the ground state which eventually becomes fragmented depending on the barrier height  $V_L$ . To compute the ground state and its subsequent real-time propagation, the many-body Hamiltonian is represented by  $128^2$  exponential discrete-variable-representation grid points in a box of size  $[-10, 10) \times [-10, 10)$ . In the main text, we calculated the many-body quantities with  $M = 8$  time-adaptive orbitals. Here we provide the convergences of the quantities discussed in this work, i.e., we show that the time-dependent many-boson wavefunction built from  $M = 8$  time-adaptive orbitals leads to numerically converged results. We have verified the convergences of the quantities with  $M = 10$  time-adaptive orbitals using  $128^2$  exponential discrete-variable-representation grid points and also, with  $M = 8$  time-adaptive orbitals using increased grid density to  $256^2$  exponential discrete-variable-representation grid points for all the barrier heights and interaction strengths  $\Lambda_0$

and  $10\Lambda_0$ . In order to demonstrate the convergences, we select the barrier height  $V_L = 13$ , the maximal barrier height for which the interference of fragmentations is appreciable, for the interaction strength  $\Lambda_0$ .

Fig. S11 represents the occupations of the first, second, third, and fourth natural orbitals, and longitudinal position variance,  $\frac{1}{N}\Delta_{\hat{X}}^2(t)$ , and transversal position variance,  $\frac{1}{N}\Delta_{\hat{Y}}^2(t)$ , at  $V_L = 13$ . The overlapping curves for all quantities with increasing grid density and number of orbitals signify that the results presented in this work are fully converged for  $M = 8$  time-adaptive orbitals with  $128^2$  exponential discrete-variable-representation grid points in a box of size  $[-10, 10) \times [-10, 10)$ .

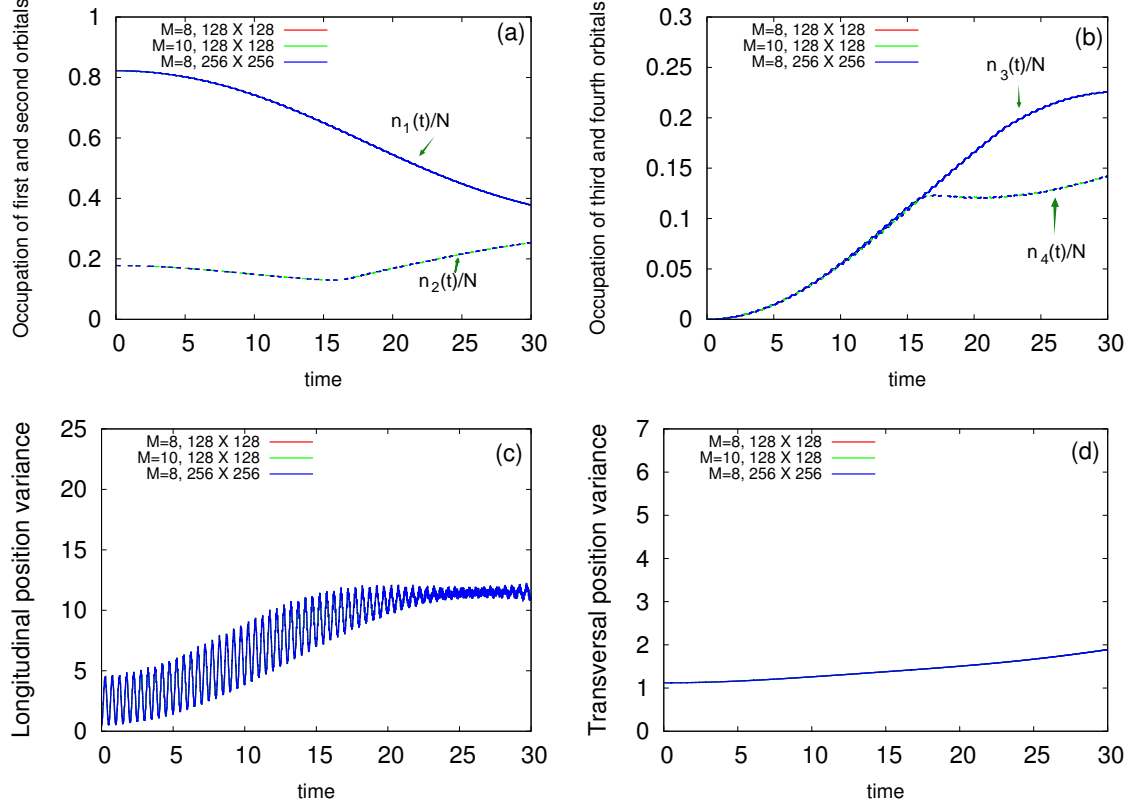


FIG. S11. Convergences of (a) the occupations of the first and second natural orbitals, (b) the occupations of the third and fourth natural orbitals, (c) many-body longitudinal position variance, and (d) many-body transversal position variance at the barrier height  $V_L = 13$  with the number of orbitals and grid points. In panel (a)[(b)], the solid lines represent the first [third] natural orbital and the dashed lines depict the second [fourth] natural orbital. The inter-boson interaction is  $\Lambda_0$  and the number of bosons  $N = 10$ . Convergences are verified using  $M = 10$  time-adaptive orbitals with  $128 \times 128$  grid points and  $M = 8$  time-adaptive orbitals with  $256 \times 256$  grid points. We show here dimensionless quantities.

---

\* [abhowmik@campus.haifa.ac.il](mailto:abhowmik@campus.haifa.ac.il)

- [1] O. E. Alon, Analysis of a Trapped Bose-Einstein Condensate in Terms of Position, Momentum, and Angular-Momentum Variance. *Symmetry* **11**, 1344 (2019).
- [2] A. U. J. Lode, C. Lévêque, L. B. Madsen, A. I. Streltsov, and O. E. Alon, Colloquium: Multi-configurational time-dependent Hartree approaches for indistinguishable particles. *Rev. Mod. Phys.* **92**, 011001 (2020).